CIRP Journal of Manufacturing Science and Technology 43 (2023) 158–169

Contents lists available at ScienceDirect

CIRP Journal of Manufacturing Science and Technology

journal homepage: www.elsevier.com/locate/cirpj

Prediction and analysis of real-time forces in novel 3D flexible rotary stretch forming of complex profiles

Jun Ma *, Sigmund A. Tronvoll, Torgeir Welo *

Department of Mechanical and Industrial Engineering, Norwegian University of Science and Technology, Trondheim 7491, Norway

ARTICLE INFO

Available online xxxx

Keywords:
3D rotary stretch bending
Real-time force
Analytical solution
Dimensional accuracy

ABSTRACT

Three-dimensional (3D), flexible rotary stretch bending is a new forming technology that enables manufacturing complex components, like 3D profiles with varying curvatures, thus addressing several limitations of conventional stretch forming processes. However, little knowledge exists about the force requirements, which in turn influence the design of process and machine tools. In this study, an analytically-based method for effective modeling of real-time forces in 3D rotary stretch bending was developed. This method considers material and geometry parameters, kinematically-controlled loading paths, as well as the workpiece-die friction effect. By forming experiments using aluminum hollow profiles with in-situ strain measurement as well as finite element analysis (FEA), the capability of the analytical model was assessed. The developed method was verified to have a similar capability to FEA for the prediction of real-time stretch strain as well as the forces of profile and tools. Based on the analytics and FEA, the developments of force components of tools during the entire forming process with pre-stretching, stretch-bending and post-stretching stages were discussed, and the friction effect on the forming forces and strain distributions were clarified. The findings facilitate analyzing force requirements and characteristics as well as can support the development of closed-loop control strategies for improved product accuracy.

Introduction

Stretch bending is widely used in manufacturing lightweight, profile-type structural components in the automobile industry owing to its high capability in mass production [1]. However, with the ongoing transformation to Industry 4.0, the metal forming sector is suffering a rapid shift from mass production towards mass customization with increased flexibility and personality to improve its competitiveness in a dynamic market as well as sustainability in the manufacturing industry [2,3]. Stretch bending is one of the most widely used processes in mass manufacturing of curved profiles due to its advantages in dimensional accuracy and productivity [4]; however, the low process flexibility and high tooling cost create challenges to meet the new demands. This puts forward a call for advanced stretch forming methods to achieve the technological transformation toward mass customization.

Conventional stretch bending processes are mainly categorized into two groups, i.e., load-controlled and kinematically-controlled methods [4,5]. The former mainly includes open-arm and rotation-arm processes, which is usually used for forming simple, symmetric geometries. The latter often includes single-rotation or double-rotation movements and is widely used for forming complex shapes. For these processes, one set of tools can generally support only one part configuration, thus resulting in low flexibility and high tooling cost. In recent years, several attempts have been put forward to improve the flexibility of conventional stretch bending processes, for example, employing a multi-point tooling strategy to replace conventional dies [6,7] and multi-point dies elastic cushions for improving dimensional accuracy [8]. Recently, Welo et al. [1] proposed a new, flexible rotary stretch bending method, in which process flexibility is achieved by increasing the rotational axes in three-dimensional (3D) space, increasing the through-process loading path control as well as applying a novel tooling design with part-specific inserts. This method enables the flexible forming of complex-shaped 2D and 3D profiles using one set of dies, providing a relatively low up-front investment for tooling in the new product development stage in particular. Although flexibility might be lower than in the multi-point forming process, the continuous tool preserves high surface quality for bent parts and maintains relatively high production efficiency. Furthermore, this method provides the flexibility for multiple loading paths, which could enable adaptive control of the process for improved product quality.

However, the fundamental knowledge of the underlying mechanisms associated with this flexible stretch bending process has

* Corresponding authors.
E-mail addresses: jun.ma@ntnu.no (J. Ma), torgeir.welo@ntnu.no (T. Welo).

https://doi.org/10.1016/j.cirpj.2023.04.001

not yet been fully established. One of the most important concerns is real-time force development, which makes it difficult to effectively design, analyze and control the process for different part configurations. The force drives the deformation in a forming operation. Effective analysis of forming forces can contribute to protecting the machines and tools, saving energy consumption, as well as improving the dimensional accuracy of formed parts. For instance, knowing real-time forces can help develop closed-loop control of the process for product quality improvement, e.g., effectively controlling springback-induced dimensional deviation and variation in bending processes [9,10]. Therefore, a strategy for modeling real-time force development will have multiple benefits for the design and control of stretch bending processes.

Although the finite element (FE) methods have been widely used in the analysis of deformation behavior, tooling design, and many other issues in metal forming processes, analytical methods offer advantages in the rapid analysis of process behavior and parameter influences, particularly in the product development stage. In addition, analytical models allow time-efficient prediction, which is of interest for industrial closed-loop control [11,12]. However, the key to realizing the value of a control strategy is that a reliable analytical model should be developed.

Up to now, many analytical studies on stretch bending have been reported. For springback analysis, for example, Yu and Johnson [13] examined the influence of axial force on bending and springback in the stretch bending of beams and obtained a basic curvature-load relationship. Since a simple, perfectly-plastic material model was used, only a rough analysis could be applied. Liu et al. [14] included friction between the profile and tools in the analysis of stretch bending by using a capstan equation, which allows evaluation of the friction influence on springback. Ma and Welo recently developed an analytical assessment method for springback assessment in a 2D rotary stretch bending process for complex profiles [1]. In this model, the strain transition between bent and straight portions is considered, thus improving the accuracy of springback prediction. In addition, some analytical research was done for analyzing cross-sectional deformation during hollow profile bending. For example, Paulsen and Welo [15] studied the cross-sectional deformation of rectangular hollow profiles in stretch bending, using an analytical model with a combination of the plasticity deformation theory and an energy method. Zhu and Stelson [16] derived analytical expressions for cross-sectional distortion in stretch bending of rectangular profiles, using the upper bound method. However, this is a purely geometrical model, giving predictions independent of material parameters. Although many analytical models could be found, these works mainly focus on springback and sectional deformation but pay little attention to the process forces acting on the workpiece and tools upon bending.

Several examples are given in the following concerning the forces in flexible forming processes. Liu and Francis [17] derived an energy-based model for analyzing the forming forces during local indentation and the shaping accuracy of the deformed part. Chang et al. [18] proposed analytical models to assess the die force during the single-point incremental forming process, by taking the contact area and the through-thickness stress into consideration. That work shows that the analytical model could provide an accurate estimation of individual force components in different directions. Grzancic et al. [11] developed an analytical model to predict the forming behavior and the forces in incremental profile forming (IPF), taking the geometry and material parameters of the tubular material into account. The model was validated by experiments and finite element (FE) simulation, allowing the force prediction during the forming processes under various parameters. Holstein et al. [19] proposed an analytical model for the prediction of process forces in incremental die forming of wires and tubes, which was confirmed by FE simulations and experiments. It was claimed that the model is suitable for designing the machine drives in process control, as well as analyzing the force variations caused by friction. The studies summarized above mainly focus on incremental forming processes for sheets and profiles. In the case of stretch bending, a simple analytical model was also derived to predict the stretch forces and force components in 2D bending [20]. However, that work is very preliminary and incapable to support effective analysis of the forming forces in advanced stretch bending processes, such as 3D flexible rotary stretch bending.

From the above review, we argue that there is a lack of analytical methods for analyzing real-time forming forces during advanced stretch bending processes. Particularly, the recently developed 3D flexible rotary stretch bending suffers from a lack of models and very few, if any, relevant studies can be found in the literature. To fill this knowledge gap, this paper aims to present an analytically-based strategy to analyze real-time forces, which may provide an effective means to interpret and use this information as input to efficiently design and control the forming process.

The remaining of this paper is organized as follows. *3D rotary stretch bending process* presents a brief introduction to the novel 3D flexible rotary stretch bending method and developed machine tools. *Analytical model of real-time forming forces* presents the analytical modeling procedure of the real-time forces in 2D/3D forming. In *Experiments and FE modelling*, the design of experiments and FE analysis for the model assessment are presented. *Results and discussion* introduces the verification of 2D/3D bending cases and discusses the force characteristics throughout the forming process. Finally, the main finding and an outlook of this research are concluded in *Conclusion and outlook*.

3D rotary stretch bending process

A new stretch bending method—called 3D flexible rotary stretch bending—was recently developed [1], aiming to enhance flexibility for manufacturing complex, customized shapes with high dimensional accuracy. Fig. 1(a) presents a schematic view of the machine design. In this method, multiple rotational axes and one translational axis are added, as shown in Fig. 1(a), and the dies with flexible geometrical configurations are used to form complex shapes, as shown in Fig. 1(b). The machine includes two sets of forming arms and each arm provides a rotational DOF in the vertical plane (*x-z* plane) controlled by Axes 2 (left arm) and 3 (right arm), and a rotational DOF (degree of freedom) in the horizontal plane (x-y plane) controlled by Axes 4 (left arm) and 5 (right arm). The rotation DOFs in the vertical and horizontal planes enable the bending deformation in their planes, in short, called 'V-bending' and 'H-bending', respectively. In addition, a translational DOF of the base platform in the *x*-direction controlled by Axis 1, enables the movement of base platforms relative to each before, during and after bending operations for stretching profile to reduce springback. As shown in Fig. 2(a), the full-scale machine was established and installed at NTNU Aluminum Product Innovation Center, in which Axes 2 and 3 employ electric servos and Axes 4, 5 and 1 use hydraulic servo actuators. Fig. 1(b) shows the die geometries and the design of rotation pivots. It can be observed that the specially designed die geometry can enable both 2D and 3D bending deformation. For both V-bending and H-bending, the eccentric pivots of dies can a certain level of stretching strain to the profile during bending operations. The machine system enables forming of both 2D and 3D part configurations with a profile length of up to 2 m. This machine can register the systematic hydraulic pressure and torques suffered by axes during forming, but cannot afford to acquire the stretch force and the force components of the clamp units and bend dies. As the stretch force and force components provided by the tools are more related to the design of the process and machine tools, they will be focused on in this research.

Compared to conventional stretch bending processes, the flexible rotary stretch bending method presented above not only facilitates

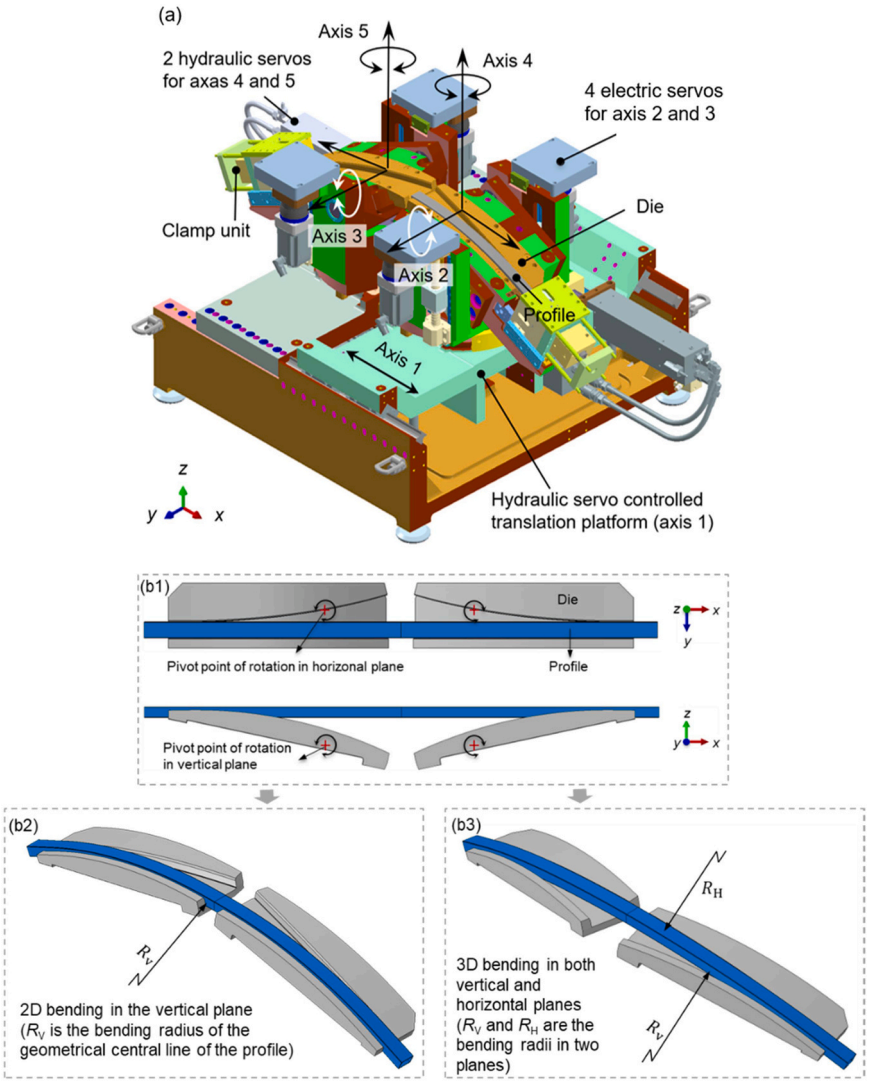

Fig. 1. Novel 3D, flexible rotary stretch bending process [1]: (a) overview of forming method and machine design; (b) illustration of 2D and 3D bending by the control of different rotation axes.

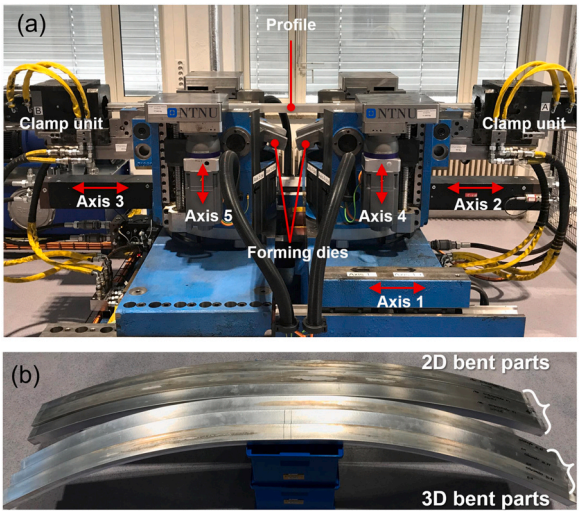

Fig. 2. Full-scale machine and formed parts: (a) 3D rotary stretch bending machine and tools; (b) experimentally formed 2D and 3D parts.

manufacturing multiple shapes and configurations with fewer part-specific tool components, but also provides multiple loading paths to control the process for better dimensional accuracy of formed parts. Therefore, the novel stretch forming method can improve process flexibility and reduce the investment of tools, particularly in the stage of product design and development.

Analytical model of real-time forming forces

An analytical approach will be used to analyze the real-time forces during the entire forming cycle. Before the development of the model, some necessary hypotheses are declared as follows:

- The cross-section of profile remains plane and perpendicular to the longitudinal axis after stretch bending.
- The stress state is uniaxial such that stresses across the thickness of members are neglected.
- Constant volume (mass conservation) principle is used for plastic deformation.
- The deformation theory of elasto-plasticity is employed.
- Large bending radius-to-depth of cross-section (Bernoulli-Navier) is assumed, and no sagging and no necking occur.

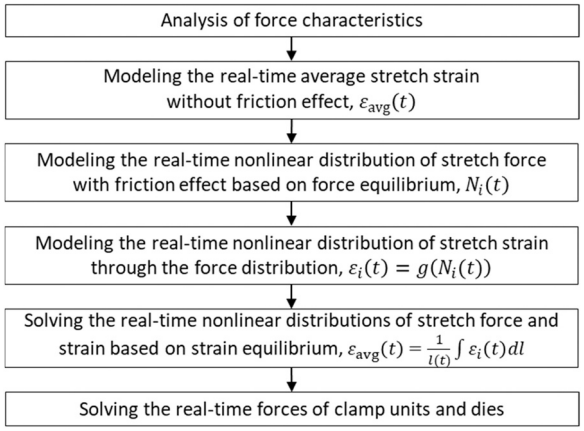

Fig. 3. Schematic flowchart of analytical modeling procedure for real-time forming forces in the 3D rotary stretch bending process.

Fig. 3 shows a schematic flowchart of the modeling procedure. First, the force characteristics during forming are analyzed, and the development of strain and axial forces of the profile is modeled based on forming kinematics. Furthermore, the distributed stretch force along the profile, considering the friction between the profile and bend die, is modeled. Then, the real-time force development at the clamp units and bend dies during the entire forming cycle is modeled analytically.

Analysis of force characteristics

The geometrical tool configuration in rotary stretch bending generally includes bent and straight portions, as shown in Fig. 1(b). Due to symmetry, one-half of the geometry is used in the following analysis. In this work, a complete process includes three stages, i.e., pre-stretching, stretch-bending, and post-stretching, is studied, and the different forming stages from the initial to the final states are demonstrated in Fig. 4(a)–(e).

Different force components prevail upon forming. In 2D bending, the forces on the profile include axial tension force, bending force, distributed contact and friction forces. Due to the kinematic characteristics of rotary draw bending, the shear force and shear strain are very minor, so they are ignored in the force analysis. Thus, the forces applied by the clamp units and bend dies can be decomposed as force components (X-direction and Z-direction) as shown in Fig. 5(a). Similarly, the force components of tools in the 3D bending case can be illustrated in Fig. 5(b), in which one more force component in y-directions exists as compared to 2D bending.

Modeling of real-time average stretch strain

To determine real-time forces, the axial stretching strain of the profile during the entire process, including the pre-stretching stage, stretch-bending stage, and post-stretching stage, needs to be determined.

Pre-stretching stage

The pre-stretch stage is a simple stretching process by controlling the movement of the base platform relative to each other. In this stage, the nominal stretching strain (ε_{avg}^{pres}) can be written as follows:

$$\varepsilon_{avg}^{pres}(t) = \frac{l(t)-l_0}{l_0} = \frac{d_{pres}(t)}{l_0},\ t \le t_1 \tag{1}$$

where the variables can be found in Fig. 4, and described as follow: l_0 is the initial effective length of the profile (clamp zones are excluded), $l(t)$ is the real-time total length of the neutral layer of the formed profile, $d_{pres}(t)$ is the real-time stretching displacement and

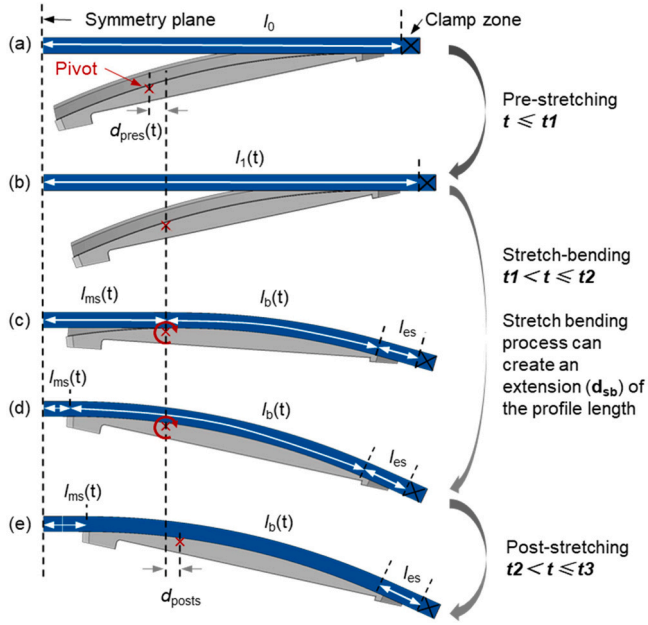

Fig. 4. Demonstration of the entire rotary stretch bending process: (a) before forming; (b) after pre-stretching; (c) during stretch-bending; (d) after stretch-bending; (e) after post-stretching.

kinematically controlled by process setting, t is the loading time, and the total pre-stretching loading time is t_1.

Stretch-bending stage

As mentioned previously, the eccentric pivots of bending dies for V-bending and H-bending would induce stretching strains to the profile. For 3D forming, both V-bending and H-bending are activated simultaneously and a synchronous mode with the same loading time was used, meaning that V-bending and H-bending are performed simultaneously. As shown in Fig. 4(a)–(c), the extension of the profile length $d_{sb}(t)$ (as shown in Fig. 4) induced in the stretch-bending stage can be expressed by:

$$d_{sb}(t) = l(t) - l_1 = [l_{es} + l_b(t) + l_{ms}(t)] - l_1,\ t_1 < t \le t_2 \tag{2}$$

where l_{es} is the length of the straight-end portion, $l_b(t)$ is the neutral layer length of the bent portion, and $l_{ms}(t)$ is the half-length of the mid-straight portion, as shown in Fig. 4. $l_b(t)$ and $l_{ms}(t)$ are time-dependent, while l_{es} keeps unchanged during forming. Once $l_b(t)$ and $l_{ms}(t)$ are solved, $d_{sb}(t)$ can thus be calculated.

In order to evaluate Eq. (2), the geometrical relationship of dies and the kinematics in rotary stretch bending is illustrated, as shown in Fig. 6. Here R_v is the bending radius of the geometrical centerline in V-bending, l_{p0} is the horizontal distance between the pivot (P_v) and the symmetry plane, which depends on the tooling configuration and the displacement of pre-stretching. l_{pv} is the distance between the pivot (P_v) and the start point of the bent portion (C), which is a constant value for a given tooling setup. $\theta(t)$ is the real-time bending angle in 2D bending. δ_v is the angle between the line CP_v and the x-y plane. As shown in Fig. 6, CP_v rotates counterclockwise during bending and can be written as $\delta_v(t) = \delta_{v0} - \alpha(t)$.

For 2D bending, based on the geometrical relationship as shown in Fig. 6(b), the length of the bent portion $l_b(t)$, and the length of the mid-straight portion $l_{ms}(t)$can be calculated as follows:

$$\begin{cases} l_b(t) = R_v\theta(t),\ t_1 < t \le t_2 \\ l_{ms}(t) = l_{p0} + l_{pv}\cos[\delta_v(t)],\ t_1 < t \le t_2 \end{cases} \tag{3}$$

For 3D bending, as the bent portion is a spatial double-curvature curve, $l_b(t)$ can be calculated by integrating the arc length,

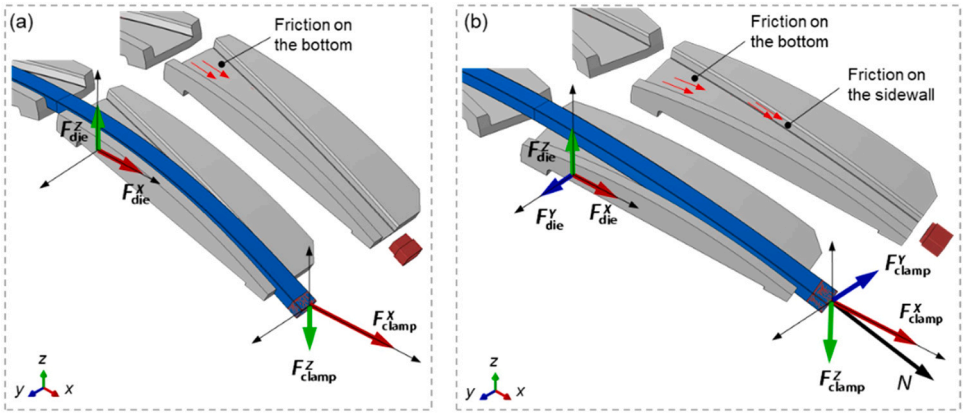

Fig. 5. Force analysis in rotary stretch bending: (a) 2D case; (b) 3D case.

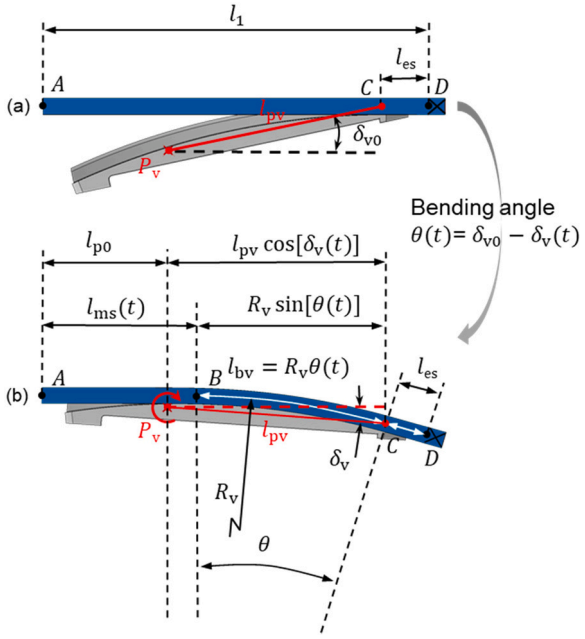

Fig. 6. Relationship between stretching displacement of profile and bending geometry during bending in the vertical plane: (a) before bending; (b) during bending.

$dl_b = \sqrt{(dx)^2 + (dy)^2 + (dz)^2}$. Due to the synchronous loading mode used in 3D bending, the lengths of straight mid portions for V-bending and H-bending are the same, meaning that Eq. (3) can also work to calculate $l_{ms}(t)$ in 3D bending. $l_b(t)$ and $l_{ms}(t)$ in 3D case can thus be written in a generalized form, as given in the following equation:

$$\begin{cases} l_b(t) = \int_0^{\theta} R_v \cos\theta(t) \sqrt{1 + \frac{(R_V \cos\theta(t))^2}{R_H^2 - (R_V \sin\theta(t))^2} + \frac{(R_V \cos\theta(t))^2}{R_V^2 - (R_V \sin\theta(t))^2}}\, d\theta, \ t_1 < t \le t_2 \\ l_{ms}(t) = l_{p0} + l_{pv}\cos(\delta_v), \ t_1 < t \le t_2 \end{cases} \tag{4}$$

where R_H is the bending radius of the geometrical centerline in H-bending, as shown in Fig. 1(b).

Accordingly, the extension of profile length $d_{sb}(t)$ can be solved. The stretch strain created in the stretch-bending stage can thus be represented by:

$$\varepsilon_{avg}^{sb}(t) = \frac{l(t) - l_0}{l_0} = \frac{d_{sb}(t)}{l_0}, \ t_1 < t \le t_2 \tag{5}$$

Post-stretching stage

In the post-stretch stage, as shown in Fig. 4, the stretching strain caused by a displacement $(d(t))$ is given as:

$$\varepsilon_{avg}^{pres}(t) = \frac{l(t) - l_0}{l_0} = \frac{d_{posts}(t)}{l_0}, \ t_2 < t \le t_3 \tag{6}$$

where t_3 is the total loading time of the entire forming cycle, and thus $(t_3 - t_2)$ is the loading time of the post-stretching stage.

In summary, the real-time average stretch strain during the entire forming process (pre-stretching, stretch-bending, and post-stretching) can be expressed as follows:

$$\varepsilon_{avg}(t) = \begin{cases} \varepsilon_{avg}^{pres}(t), \ t \le t_1 \\ \varepsilon_{avg}^{pres}(t_1) + \varepsilon_{avg}^{sb}(t), \ t_1 < t \le t_2 \\ \varepsilon_{avg}^{pres}(t_1) + \varepsilon_{avg}^{sb}(t_2) + \varepsilon_{avg}^{pres}(t), \ t_2 < t \le t_3 \end{cases} \tag{7}$$

Modeling of stretch force evolution with friction effect

In stretch bending of a long profile part, one-dimensional state deformation along the longitudinal direction of the profile. Once the average stretch strain is determined, the average stretch force $(N_{avg}(t))$ of the formed profile can be represented as follows:

$$N_{avg}(t) = A_{sec}\sigma_{avg} = Af(\varepsilon_{avg}) \tag{8}$$

where A_{sec} is the nominal cross-sectional area of the profile, σ is the engineering stress and can be represented by the material's constitutive model $\sigma = f(\varepsilon)$.

It is noted that the average stretch force $(N_{avg}(t))$ defines the uniformly distributed axial forces along the formed profile under the assumption of zero friction. In the actual forming process, however, the stretch strain is nonuniformly distributed along the formed profile due to friction between the profile and bend dies. This leads to a nonuniform distribution of the axially stretch force along the profile, which cannot be captured by Eq. (8). Thus, a correction needs to be made to describe the nonuniform force distribution caused by friction.

Fig. 7 illustrates the schematic view of the friction force in 2D bending. In 2D bending, there is one friction couple between the die bottom and the profile (in short 'bottom friction'), as shown in Fig. 5(a). For straight portions (AB and CD), the contact pressure is much smaller than that in the bent portion, the associated friction force is much smaller. It is assumed that the straight portions are not affected by bending stiffness and the strain transition between bent and unbent portions is neglected. Under this assumption, the stretch force is uniformly distributed, and the forces at A, B, C, and D yield the equations as follows: $N_A = N_B$ and $N_C = N_D$.

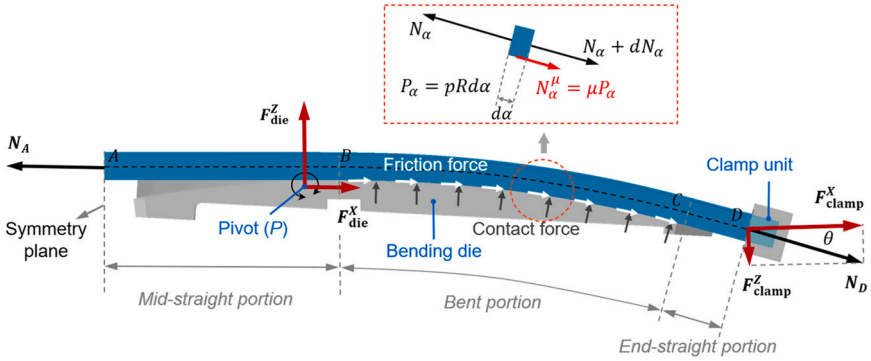

Fig. 7. Distribution of friction force on the profile during the rotary stretch bending process.

For the bent area, to describe the friction between tools and workpiece, the classical Coulomb friction law, $\tau = \pm\mu p$, was employed, in which μ is a constant friction coefficient, and τ and p are the shear stress and contact pressure between the tool and the formed profile, and the sign is determined by the relative sliding direction. Fig. 7 shows the schematic view of the friction force acting on the profile in 2D bending, where an element $d\alpha$ at an arbitrary position (section-α) is taken for analysis. $P_\alpha = pRd\alpha$ represents the normal contact force, and $N_\alpha^\mu = \mu P_\alpha$ is the friction force. The equilibrium equations of the forces in the circumferential and radial directions can be obtained as follows:

$$\begin{cases} N_\alpha + dN_\alpha + \mu pRd\alpha = N_\alpha, & \text{circumferential direction} \\ 2N_\alpha \sin(d\alpha/2) = pRd\alpha, & \text{radial direction} \end{cases} \tag{9}$$

where N_α denotes the axial force at the Section-α, and R is the tool radius.

By solving the above equilibrium equations, the axial force (N_α) at an arbitrary section-α in the bent portion can be obtained as follows:

$$N_\alpha = N_B \exp(-\mu\alpha), \text{ or, } N_\alpha = N_A \exp(-\mu\alpha) \tag{10}$$

In 3D bending, in addition to the 'bottom friction' in 2D bending, another contact pair between the side surfaces of bend die and profile also comes in profile (in short described 'side friction'), as shown in Fig. 8. The two contact pairs could be activated simultaneously in this study. For each type of friction, the friction forces that are perpendicular to the stretching direction are neglected. Thus, the 'bottom friction' force and 'side friction' forces are in the same direction as the axial force during forming. According to the superposition principle, the friction forces could be considered in the analysis of forming forces in 3D bending. Following this, the axial force distribution as described by Eq. (10) can be extended to a more generalized 3D forming processes, as shown in the following:

$$N_{\alpha,\beta}(t) = N_A(t)\exp(-\mu\alpha)\exp(-\mu\beta) \tag{11}$$

where $N_{\alpha,\beta}(t)$ is the axial force at arbitrary section-(α, β) in 3D bending (α and β are the angles of V-bending and H-bending, respectively), as shown in Fig. 8.

Accordingly, the real-time distribution of stretch force along the entire profile can be represented by a function of the axial force at the mid-section ($N_A(t)$), as given by:

$$N_i(t) = \begin{cases} N_A(t), & \text{from A to B} \\ N_A(t)\exp(-\mu\alpha)\exp(-\mu\beta), & \text{from B to C} \\ N_A(t)\exp(-\mu\theta)\exp(-\mu\varphi), & \text{from C to D} \end{cases} \tag{12}$$

where $N_i(t)$ is the real-time distribution of stretch force, in which the subscript 'i' represents the section location along the profile.

Then, the stretch stress ($\sigma_i(t)$) at Section-i can be calculated as follows:

$$\sigma_i(t) = N_i(t)/A_{sec} \tag{13}$$

where A_{sec} is the nominal cross-sectional area at Section-i.

Once the stretch stress is known, the stretch strain at Section-i can be calculated by an inverse function of the material constative model ($\varepsilon = f^{-1}(\sigma)$). As a results, the nonuniformly distributed stretch strain considering the friction effect along the entire profile can be represented by:

$$\varepsilon_i(t) = f^{-1}(N_i(t)/A_{sec}) \tag{14}$$

Furthermore, the average stretch strain of the formed profile can be calculated by integrating the nonuniform strain distribution and divided by the total length of the profile, which is equal to the average stretch strain with zero friction (as given in Eq. (7)). This leads to the following equilibrium equation:

$$\frac{1}{l(t)}\int_A^D f^{-1}\left(\frac{N_i(t)}{A_{sec}}\right)dl = \varepsilon_{avg}(t) \tag{15}$$

where $l(t)$ is the real-time total length of the neutral layer of the formed profile. It is kinematically controlled by process setting and has been calculated in *Modelling of real-time average stretch strain*. A detailed form of Eq. (15) is obtained by substituting $N_i(t)$ by Eq. (12):

$$\frac{1}{l(t)}\left[\int_A^B f^{-1}\left(\frac{N_A(t)}{A_{sec}}\right)dl + \int_B^C f^{-1}\left(\frac{N_{\alpha,\beta}(t)}{A_{sec}}\right)dl + \int_C^D f^{-1}\left(\frac{N_C(t)}{A_{sec}}\right)dl\right] = \varepsilon_{avg}(t) \tag{16}$$

in which $N_{\alpha,\beta}(t)$ and $N_C(t)$ have been represented by a function of $N_A(t)$, as given in Eq. (12).

By solving Eq. (16), the stretch force at Section-A ($N_A(t)$) can be obtained, and accordingly, the distributions of stretch force and variable stretch strain due to friction can be solved analytically by Eqs. (12) and (14).

Modeling of real-time forming forces

As shown in Fig. 5, the axially stretch force at section-D can be decomposed in the global coordinate system, as given in the following:

$$F_D^X(t) = N_D(t)\cos\varphi\cos\theta \tag{17a}$$

$$F_D^Y(t) = N_D(t)\sin\varphi \tag{17b}$$

$$F_D^Y(t) = N_D(t)\cos\varphi\sin\theta \tag{17c}$$

where F_D^X, F_D^Y and F_D^Z are the force components in X-, Y-, and Z-directions, respectively.

Accordingly, the real-time force components F_{clamp}^X, F_{clamp}^Y, and F_{clamp}^Z (as shown in Fig. 5) applied by the clamp unit can be obtained, as given in the left column in Table 2. By an equilibrium analysis of the entire forming system, the real-time force components F_{die}^X, F_{die}^Y,

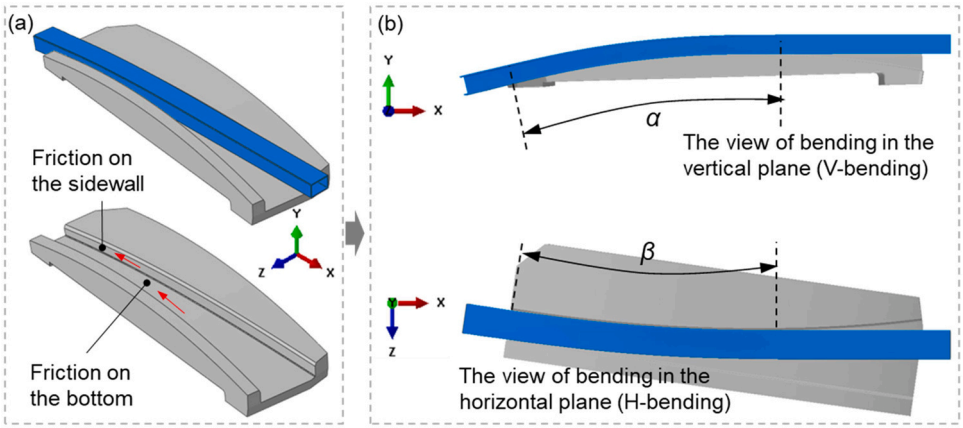

Fig. 8. Schematic of the friction in 3D bending: (a) 'bottom friction' and 'side friction'; (b) angles of V-bending and H-bending at arbitrary section.

and F_{die}^{Z} (as shown in Fig. 5) applied by the bend die can be obtained, as given in the right column in Table 2.

Experiments and FE modeling

Rotary stretch bending experiments

To verify the real-time force model developed in *Analytical model of real-time forming forces*, both 2D and 3D rotary stretch bending experiments were performed on the full-scale machine using AA6082-T4 extruded rectangular hollow profiles with nominal cross-sectional dimensions of 60 mm × 40 mm × 3 mm (width × depth × thickness). The basic mechanical properties of the profiles were measured by uniaxial tensile tests in a previous study [1], and Young's modulus is E = 69,982 MPa, initial yield strength is σ_0 = 146 MPa, and ultimate tensile strength is σ_{uts} = 266 MPa. The nominal stress-strain curve is fitted by using the following equations:

$$\sigma = f(\varepsilon) = \begin{cases} E\varepsilon, \text{ elastic} \\ K(\varepsilon_0 + \varepsilon)^n, \text{ plastic} \end{cases} \quad (20)$$

where the fitting parameters are: n = 0.21, K = 405 MPa and ε_0 = 0.004.

In the experiments, the loading mode 'pre-stretch → stretch-bending → post-stretch' was used to control the forming process. For each case, three repeated tests were conducted. The experimental parameters are given in Table 1. The initial length of the profiles for forming is 1900 mm. The radius of bend die surface (bent portion) and the angle for V-bending are 1807 mm and 24.6 deg., respectively. The radius of bend die surface (bent portion) of the and the angle for H-bending are 2905 mm and 15 deg., respectively. As shown in Fig. 2(d), the length of the mid-straight portion is l_{ms} = 82.20 mm, the length of the end-straight portion is l_{ess} = 106.30 mm. In the forming process, the profile was firstly pre-stretched by 1.8% nominal stretch strain with 21.11 s, subsequently bent with 15.07 s, and then post-stretched by 2% nominal stretch strain to the final position with 21.11 s. In the forming experiments, the tools and profiles were not lubricated (dry friction condition). The formed 2D and 3D parts in the experiments are shown in Fig. 2(b).

Real-time in-situ strain measurement

An indirect way was used to analyze the real-time stretching force during forming. In this method, the real-time in-situ stretch strain of the profile during forming is measured and then the force can be calculated by using the measured strain and the stress-strain relationship. To this end, the experiments were designed to measure the real-time axial strain of the profile's mid-section, as shown in Fig. 9(a). Instron 2620–601 dynamic extensometer (gauge length: 12.5 mm, travel displacement: ± 5.0 mm) was used. As shown in Fig. 9(b) and (c), the extensometer was fixed on the side surface (locally roughened by grind papers to avoid sliding) at the middle of the profile using rubber bands. QuantumX MX1645B amplifier and CatmanAP were used to record and analyze the real-time data, as shown in Fig. 9(d). Once the real-time strain of the mid-section of the profile is obtained, the real-time stretching force at the mid-section can be calculated by Eq. (19). Furthermore, the non-uniform distribution of axial forces and strains along the profile can be solved by the analytical method developed in *Analytical model of real-time forming forces*.

FE modeling of rotary stretch bending

As the experiments can only provide the strain and force in the middle of the profile, the FEA was also used to assist verify the real-time force components of tools predicted by the analytical model as well as analyze the strain distributions in the forming process. A FE model was built based on Abaqus R2017x using explicit solver, as shown in Fig. 10. A half CAD model was used due to symmetry to save computational time. The tools were modeled as rigid bodies and meshed by R3D4 elements (4 node 3D surface), and the hollow profile was modeled as solid deformable body and meshed by C3D8R elements (8 node 3D brick elements, reduced integration) with a size of

Table 1
Experimental parameters for 2D and 3D bending processes controlled by 'pre-stretching → bending → post-stretching' loading mode.

Parameter type	Description	2D bending	3D bending
Bending related parameters	V-bending angle [deg.]	24.6	24.6
	Radius of die surface for V-bending [mm]	1807	1807
	V-bending-induced stretching strain	2%	2%
	H-bending angle [deg.]	/	15
	Radius of die surface for H-bending [mm]	/	2950
	H-bending-induced stretching strain	/	1%
Stretching related parameters	Pre-stretching strain	1.8%	1.8%
	Post-stretching strain	2%	2%

Table 2
Force components of the claim unit and bend dies during rotary stretch bending.

Clamp unit	Bend die
$F^X_{clamp} = \begin{cases} N(t), & t \le t_1 \\ F^X_D(t), & t_1 < t \le t_3 \end{cases}$ (18a)	$F^X_{die} = \begin{cases} 0, & t \le t_1 \\ N_A(t) - F^X_D(t), & t_1 < t \le t_3 \end{cases}$ (19a)
$F^Y_{clamp} = \begin{cases} 0, & t \le t_1 \\ F^Y_D(t), & t_1 < t \le t_3 \end{cases}$ (18b)	$F^Y_{die} = \begin{cases} 0, & t \le t_1 \\ -F^Y_D(t), & t_1 < t \le t_3 \end{cases}$ (19b)
$F^Z_{clamp} = \begin{cases} 0, & t \le t_1 \\ F^Z_D(t), & t_1 < t \le t_3 \end{cases}$ (18c)	$F^Z_{die} = \begin{cases} 0, & t \le t_1 \\ -F^Z_D(t), & t_1 < t \le t_3 \end{cases}$ (19c)

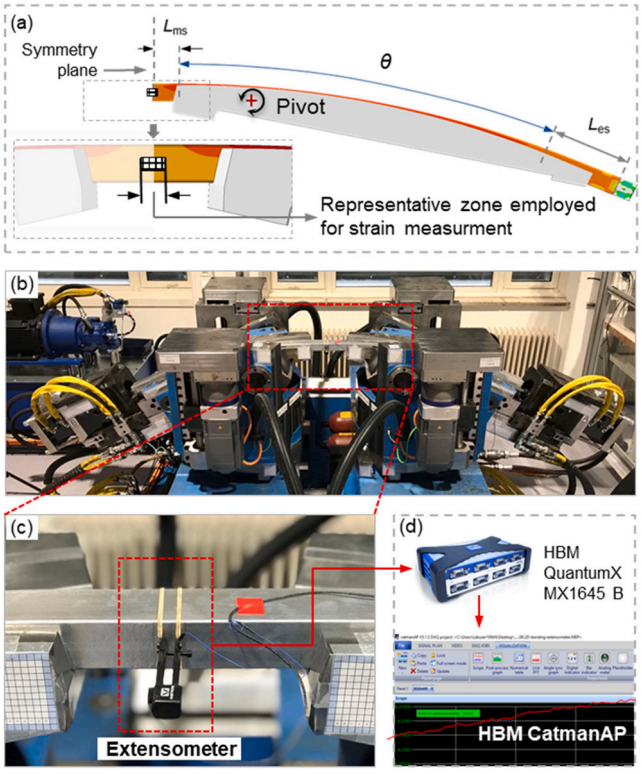

Fig. 9. Real-time axial strain measurement in the middle of the profile during forming: (a) schematic illustration of real-time axial strain measurement of the formed profile; (b) forming process with real-time strain measurement; (c) extensometer installed at the symmetry position (mid-section) of the profile; (d) data acquisition and processing.

4 × 3 × 1 mm and hourglass control. The friction between the profile and dies was described by Coulomb friction law, and the friction coefficient was set as 0.2 due to the dry friction in the forming experiments [14]. Hooke's law and J_2 plasticity model calibrated by the uniaxial tensile tests were used to describe the material behavior in simulations. The kinematical boundaries were set as well as possible to represent those in the experimental forming processes.

Results and discussion

Prediction and analysis of real-time strain

Fig. 11 shows the experimentally measured real-time strain curves at the mid-section of the profile and the strain curves predicted by the developed analytical model and FEA. It is noted that the analytical model developed in *Analytical model of real-time forming forces* was programmed based on Matlab 2021b, and the friction coefficient in analytical calculations was set as $\mu = 0.2$

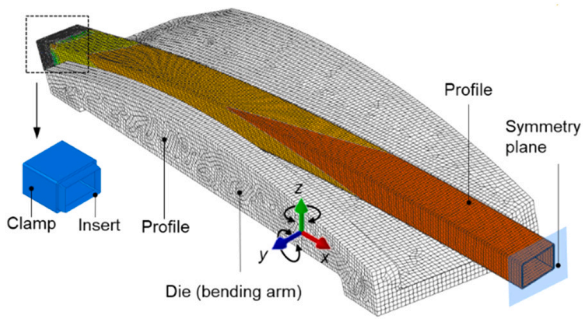

Fig. 10. FE modeling of rotary stretch bending.

(as same as FEA). As the experimental and analytical results are engineering strain curves, the logarithmic strains predicted by FEA were converted to engineering strain curves and plotted in Fig. 11, and the FEA strain curve is an average value of the strains at the four representative zones on the top, bottom, and sidewalls of the profile, as illustrated in Fig. 12. For comparison, the average stretch strain curve (ε_{avg}) calculated by pure kinematic relationship without friction are also plotted in Fig. 11.

First, the experimentally measured real-time strain development at the mid-section during forming is analyzed. In the 2D case, it can be found from Fig. 11 (a) that the strain accumulated in the pre-stretch stage is about 1.6%, which is very close to the average stretch strain of 1.8% (as given in Table 1), as this stage is a uniform stretching process with no friction effect. In the stretch-bending stage, however, the measured strain (about 5.1%) is much higher than the average strain of 3.8%. At the end of the entire forming process, the difference between the measured strain (7.6%) and the average strain value (5.8%) is more significant. The difference between measured strains in the actual forming process and the theoretical ones shows a significant nonuniform deformation along the profile, as shown in Fig. 11 (a). Such nonuniform deformation is primarily due to the friction effect. In the post-stretch stage, although the contact area is not changed, the distributed varying friction forces continue to cause nonuniform deformation. In the 3D case, due to the increased straining level in the stretch-bending stage as well as the friction between profile sidewall and dies, the more pronounced nonuniform distribution of strain can be found in Fig. 11 (b), leading to more significant difference between the measured strains and the average strains (see Fig. 11 (b)).

Furthermore, the strain curves obtained by the analytical model, FEA and experiments are compared and discussed. In the 2D case, as shown in Fig. 11 (a), the analytical curve is almost identical to the FEA curve throughout the forming process, and both show perfect agreement with the experimental strain curve. In the 3D case, as shown in Fig. 11 (b), the FEA and analytical curves are very similar with a very small difference in the stretch-bending stage and at the end of the post-stretch stage. Compared with experimental results in 3D forming, FEA can accurately reproduce real-time strain development in the pre-stretch and stretch-bending stages. However, the FEA strain curve is a slightly lower than the experimentally recorded one in the post-stretch stage. As compared to 2D forming, the prediction accuracies of both analytical model and FEA are slightly decreased. In 3D forming, the deformation behavior is more complex, for example, more complex friction effect, increased strain transition phenomenon between the bent and unbent portions, etc. The more complex deformation might be the reason for more scattered experimental data at the post-stretching stage of 3D forming (see Fig. 12), as well as for the loss of prediction accuracies of the FEA and the analytical model as compared to the 2D forming. In both analytical calculation and FEA, a constant friction coefficient of 0.2 was used, without considering the variation of friction coefficient

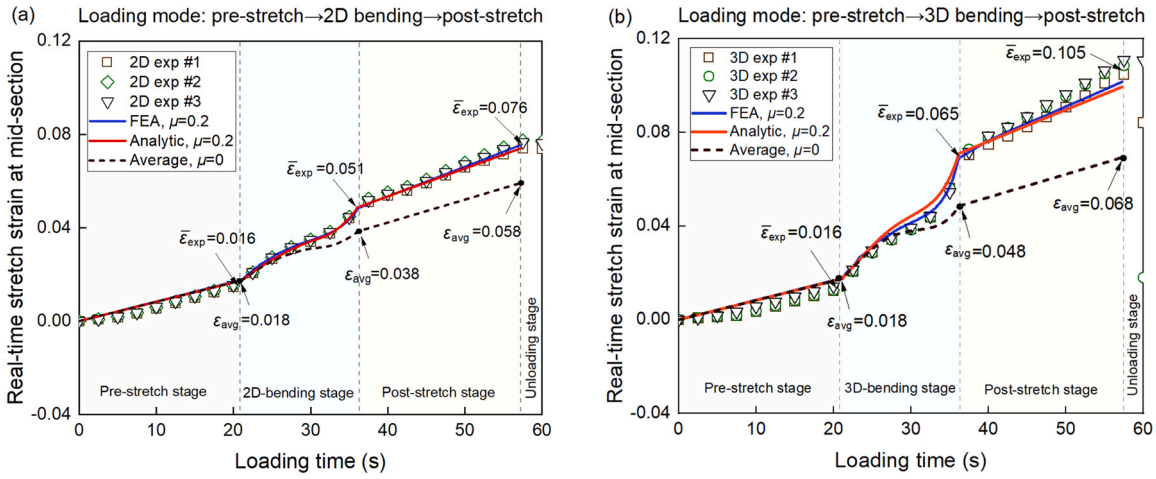

Fig. 11. Experimentally measured and FEA predicted real-time strains at the mid-section of the profile: (a) 2D bending; (b) 3D bending.

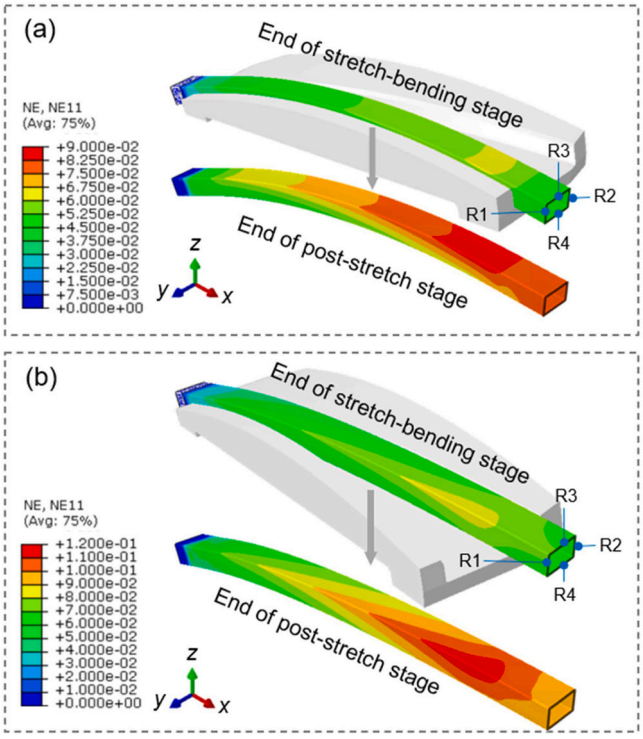

Fig. 12. Axial nominal strain distribution during forming: (a) 2D bending; (b) 3D bending.

caused by the dynamic change in contact conditions in the actual processes. In addition, as shown in Fig. 12, a strain transition phenomenon exists between the bent and unbent (straight) zones, which can be captured by FEA but is not considered in the analytical model. Both above two aspects can result in a deviation between analytical calculations and FEA as well as experiments. From the above discussion, it can be found that the analytical model has similar accuracy to FEA, providing an effective estimation of real-time strain development at the mid-section in 2D and 3D forming.

In addition, the analytical model can not only provide the analysis of real-time strain development during the forming process but also allows the calculation of strain and stress distribution over the entire formed profile. Using the 2D case as an example, the strain and stress distributions are discussed. Fig. 13 (a) and (b) show the nominal axial stretch strain distribution and the nominal axial stress distribution obtained by analytical calculation along the length of the profile, respectively. For comparison, the nominal strain and stress distribution along the geometrical centerline of the profile obtained from FEA are plotted. It can be seen that the analytical results and FEA are quite close, particularly in the bent position. For the transition area close to the clamp area, a relatively larger deviation between the analytical results and FEA results can be found, which can be caused by the highly nonuniform deformation in this transition area. The FEA results extracted from geometrical centerline may not accurately represent the average stretch strain in the profile's section. Overall, the analytical model can provide an equivalent capability to FEA for predicting the strain and stress distribution over the profile length. Such information will contribute to a more accurate analysis of springback behavior as it enables taking the nonuniform stress distribution over the length of the profile into account, rather than treating bending deformation along the profile length as uniformly distributed in the conventional springback analysis methods.

Prediction and analysis of real-time forces

As the analytical method has been confirmed to have similar accuracy to FEA in predicting the real-time stretch strain at the mid-section of the profile, the stretch forces predicted by the two approaches would be more similar due to the flattened work-hardening of the material. As shown in Fig. 14, the two force curves in 2D forming are almost the same, and the maximum deviation in 3D bending is as lower as 1.5% of the FEA value.

Furthermore, the force components (as indicated in Fig. 5 in *Analysis of force characteristics*) applied by the clamp units and bend dies during forming are analyzed. Fig. 15 gives the force components of the clamp units and bend dies, provided by the analytical method and FEA. It can be observed that the force components solved by the analytical model show high agreement with the FEA results in the entire 2D and 3D forming processes. Therefore, the analytical model with friction considered can provide a very similar prediction capability as FEA in the analysis of the real-time stretch force at the profile's mid-section as well as the real-time force components applied by the tools during the entire forming processes.

Based on analytical calculations and FEA, the development of different force components during forming is discussed. In the forming processes, the pre-stretch stage is a simple step with uniaxial tension, so the force development in the stretch-bending and post-stretching stages is particularly discussed. For the clamp unit, as shown in Fig. 15 (a), F^{X}_{clamp} is much higher than F^{Y}_{clamp}, as F^{X}_{clamp} is the main contributor to provide horizontal stretching to the profile. In the stretch-bending stage, F^{X}_{clamp} is increased initially and then

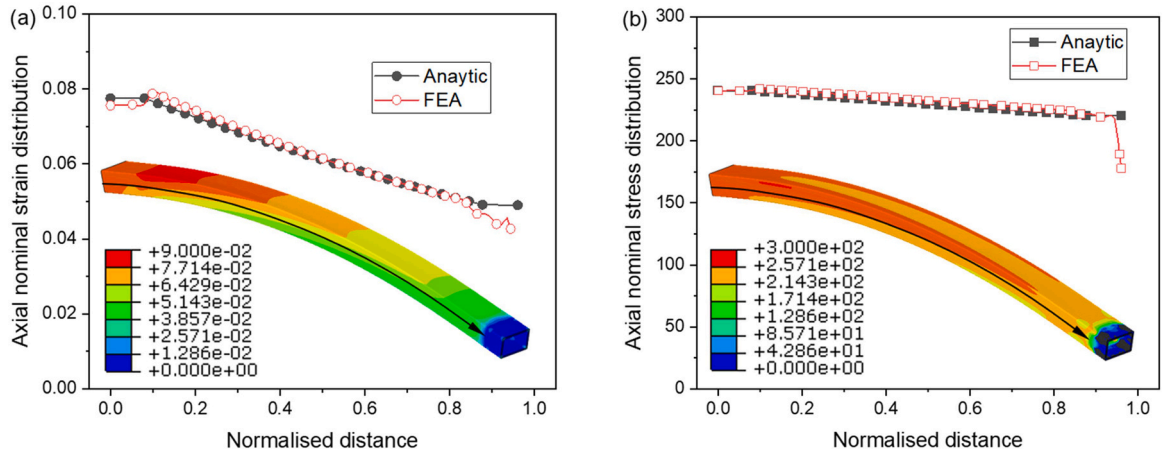

Fig. 13. Analytical strain and stress distribution over the entire formed profile at end of the 2D forming process: (a) axial nominal strain; (b) axial nominal stress.

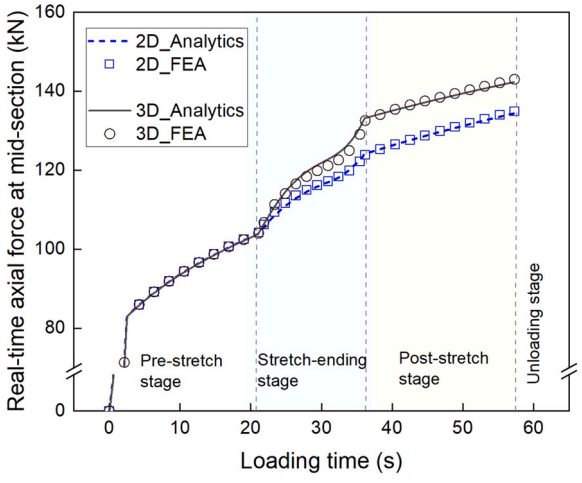

Fig. 14. Real-time stretch forces at the profile mid-section, obtained by FEA and analytics.

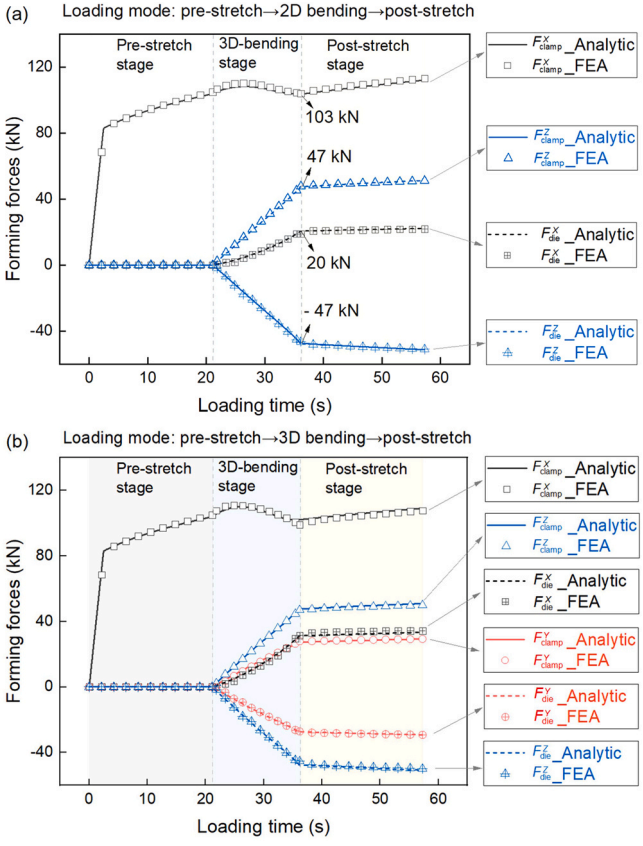

Fig. 15. Real-time force components applied by the clamp units and bend dies during forming: (a) 2D bending; (b) 3D bending.

presents a slight decrease, and F^{Z}_{clamp}presents a significant increase. When bending angle is increased during forming, the increased contact area between the bend die and profile makes F^{X}_{clamp} present such a nonlinear trend in the stretch-bending stage. The increased bend angle and accordingly increased friction force also led to an increase in F^{X}_{die} at the same time. In the post-stretch stage, all the force components of the clamp unit and bend die slightly increase. During post-stretching, the contact area between the bend die and profile is as same as that at the end of the stretch-bending stage; however, the increased stretching deformation makes the stretch force of profile and the contact and friction forces slightly increase. In 3D forming, as shown in Fig. 15 (b), the overall force characteristics are similar to the 2D forming, except for one more force component in y-direction induced by V-bending. The die curvature of V-bending is smaller than H-bending so the magnitudes of force components in y-direction is smaller than those in z-direction caused by H-bending.

Friction effect on the forming forces

The forming forces does not only depend on the material property and strain level but also are sensitive to the friction between tools and workpiece. In this study, using the verified analytical model with changing the value of friction coefficient from 0 to 0.3, the effect of friction on the forming forces have been explored. Fig. 16 (a) and (b) demonstrate the forces under different friction coefficients for 2D and 3D bending processes, respectively. In the 2D bending, with the increase of friction coefficient, the force components of clamp unit in the X-direction (F^{X}_{clamp}) and Z-direction (F^{Z}_{clamp}) decreases, while the force of the bend die in the two directions increases. The friction effect on the forces in the X-direction is more significant than the forces in the Z-direction. For a more detailed analysis, the X-directional forces at the end of the forming process is applied as a reference to quantitatively study the friction effect. Increasing the friction coefficient from 0 to 0.3 for 2D bending, the F^{X}_{clamp} is decreased by about 6.24%, while the F^{X}_{die} is increased by 2.33 times. The friction effect on the force components in the X-direction

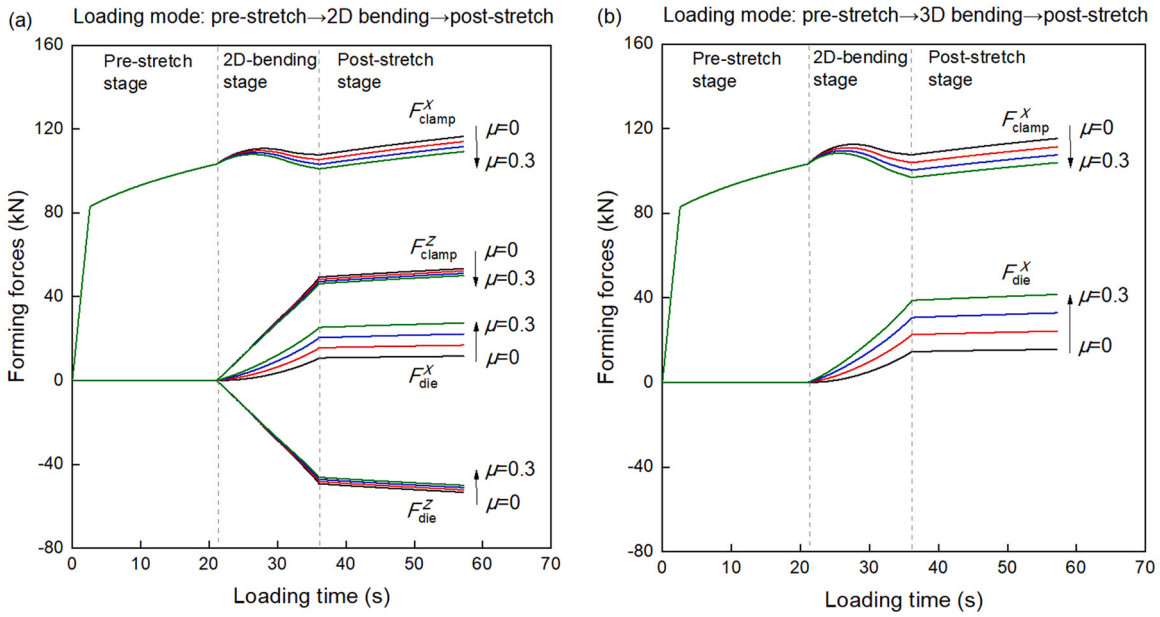

Fig. 16. Effect of friction on the forming forces: (a) 2D bending; (b) 3D bending.

is more significant than other force components for both clamp units and dies. For the 3D bending, the X-directional force components of the clamp unit and bend die are plotted in Fig. 16 (b). The overall characteristic of friction effect on the forming forces in 3D forming are similar to the 2D bending. When taking the X-directional forces at the end of forming process for a detailed analysis, it can be found that, when the friction coefficient is increased from 0 to 0.3, the F^X_{clamp} is decreased from by about 10%, while the F^X_{die} is increased by about 2.66 time. Thus, it could be concluded that the influence of friction on the forming forces in 3D bending is more significant than the 2D bending. As discussed in *Modelling of stretch force evolution with friction effect*, the 3D bending process include two contact pairs, i.e., 'bottom friction' and 'side friction', which make the friction behavior during 3D bending is more pronounced than the 2D bending case.

In addition, the variation of friction present significant influence on the strain distribution over the profile length. As shown in Fig. 17 (a), under an ideal condition without friction ($\mu = 0$), the nominal axial strain distribution on the bent portion along the profile length is very uniform. Except for the transition area between bent and unbent portions, the axial strain distribution in each section is almost same. However, under the practical forming cases with friction, the axial strain distribution presents a nonuniform characteristic. With the increase of friction coefficient from $\mu = 0.1$–0.3, the nonuniformity of axial strain along the profile length becomes more pronounced. Looking into the strain of the upper flange, the maximum axial strain under $\mu = 0.1$ is about 0.07, however, the maximum axial strain under $\mu = 0.3$ can be up to about 0.1. For 3D bending, as shown in Fig. 17 (b), due to the increased friction effect caused by 'bottom friction' and 'side friction', the friction-induced strain

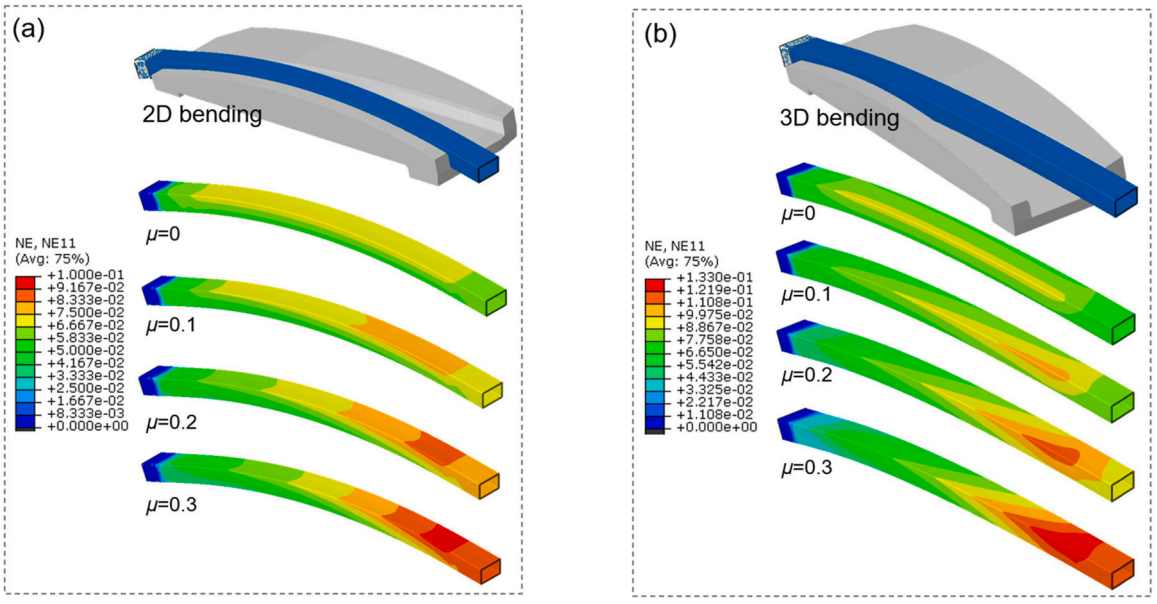

Fig. 17. Effect of friction on the strain distribution: (a) 2D bending; (b) 3D bending.

nonuniformity along the profile length becomes more significant as compared to 2D bending. Thanks for the V-bending and H-bending in the vertical and horizontal planes, the overall strain distribution is more complex, and the maximum strain locates at the corner extrados of two bending directions.

Friction not only influence the forming force and strain distribution but also affects the surface quality of the formed parts. In practical production, to obtain a better surface quality, the contact surfaces are normally lubricated. However, the lubrication could reduce the friction effect and further change the magnitudes the force components of the clamp units and bend dies, which needs to be considered in the design of production processes. The analytical force model developed herein could provide an effective and accurate approach to analyze the forces of the clamp units and bend dies, thus supporting the efficient design of the manufacturing process from the perspective of the forming forces.

Conclusion and outlook

Effective and efficient prediction and analysis of real-time forming forces is of significance to the development of products, processes, and machine tools in forming processes. In this study, an analytical method for rapid, cost-effective prediction of real-time forces in newly developed 3D rotary stretch forming for manufacturing complex profile components is presented. This analytical method considers the kinematically controlled loading path, material and geometry parameters, and particularly the workpiece-die friction for modeling the complex nonuniform deformation behavior and thus improving the analysis accuracy. Using experiments and FEA under a complex loading path including pre-stretching, stretch-bending and post-stretching, the analytical model was assessed to have a similar capability to FEA for the prediction of real-time stretch strain and force on the profile as well as the force components of the tools. As compared to FEA, the maximum deviation of the analytical calculations for forming forces is about 1.5%. Based on analytical calculations and FEA, the development characteristics of force components of the clamp units and bend dies were clarified and the influence of friction on the forming forces and strain distributions were revealed, providing an in-depth understanding of the force behavior in the entire process. Due to the high solving efficiency, the developed analytical model can facilitate effective analysis of force requirements in the design of process and machine tools. The advantages of accuracy, efficiency and the consideration of complex load paths also offer a potential for the development of closed-loop control strategies for improving product quality in rotary stretch bending processes.

CRediT authorship contribution statement

Jun Ma: Conceptualization, Methodology, Investigation, Formal analysis, Writing – original draft, Writing – review & editing. **Sigmund A. Tronvoll:** Methodology, Investigation, Writing – review & editing. **Torgeir Welo:** Methodology, Investigation, Writing – review & editing.

Declaration of Competing Interest

The authors declare that they have no known competing financial interests or personal relationships that could have appeared to influence the work reported in this paper.

Acknowledgments

The authors gratefully acknowledge the financial support from Norwegian University of Science and Technology (NTNU), NTNU Aluminum Product Innovation Center (NAPIC), and the TaFF project (No.: 317777) and AdaptAl project (No.: 314054) sponsored by Research Council of Norway. In addition, the authors would like to thank Dr. SQ Wang at NTNU for his help in strain measurement.

References

[1] Ma, J., Welo, T., 2021, Analytical springback assessment in flexible stretch bending of complex shapes. International Journal of Machine Tools and Manufacture, 160:103653. https://doi.org/10.1016/j.ijmachtools.2020.103653.
[2] Yang, D.Y., Bambach, M., Cao, J., Duflou, J.R., Groche, P., et al., 2018, Flexibility in metal forming. CIRP Annals – Manufacturing Technology, 67/2:743–765. https://doi.org/10.1016/j.cirp.2018.05.004.
[3] Cao, J., Banu, M., 2020, Opportunities and challenges in metal forming for lightweighting: review and future work. Journal of Manufacturing Science and Engineering, 142:1–24. https://doi.org/10.1115/1.4047732.
[4] Vollertsen, F., Sprenger, A., Kraus, J., Arnet, H., 1999, Extrusion, channel, and profile bending: a review. Journal of Materials Processing Technology, 87/1–3:1–27. https://doi.org/10.1016/S0924-0136(98)00339-2.
[5] Zhai, R., Ding, X., Yu, S., Wang, C., 2018, Stretch bending and springback of profile in the loading method of prebending and tension. International Journal of Mechanical Sciences, 144:746–764. https://doi.org/10.1016/j.ijmecsci.2018.06.028.
[6] Liang, J.C., Gao, S., Teng, F., Yu, P.Z., Song, X.J., 2014, Flexible 3D stretch-bending technology for aluminum profile. International Journal of Advanced Manufacturing Technology, 71/9–12:1939–1947. https://doi.org/10.1007/s00170-013-5590-9.
[7] Liang, J., Chen, C., Li, Y., Liang, C., 2020, Effect of roller dies on springback law of profile for flexible 3D multi-point stretch bending. International Journal of Advanced Manufacturing Technology, 108/11–12:3765–3777. https://doi.org/10.1007/s00170-020-05655-6.
[8] Cherukupally, S., Konka, P., Venkata Reddy, N., 2022, Enhancement of accuracy in multi-point stretch forming: cushion stretching. Manufacturing Letters, 33:205–213. https://doi.org/10.1016/J.MFGLET.2022.07.027.
[9] Geiger, M., Sprenger, A., 1998, Controlled bending of aluminium extrusions. CIRP Annals – Manufacturing Technology, 47/1. https://doi.org/10.1016/s0007-8506(07)62817-0.
[10] Zhu, H., Stelson, K.A., 2003, Modeling and closed-loop control of stretch bending of aluminum rectangular tubes. Journal of Manufacturing Science and Engineering, Transactions of the ASME, 125/1:113–119. https://doi.org/10.1115/1.1536659.
[11] Grzancic, G., Löbbe, C., Ben Khalifa, N., Tekkaya, A.E., 2019, Analytical prediction of wall thickness reduction and forming forces during the radial indentation process in incremental profile forming. Journal of Materials Processing Technology, 267/2018: 68–79. https://doi.org/10.1016/j.jmatprotec.2018.12.003.
[12] Welo, T., 2013, Intelligent manufacturing systems: controlling elastic springback in bending. IFIP Advances in Information and Communication Technology, 397/Part 1: 460–466. https://doi.org/10.1007/978-3-642-40352-1_58.
[13] Yu, T.X., Johnson, W., 1982, Influence of axial force on the elastic-plastic bending and springback of a beam. Journal of Mechanical Working Technology, 6/1:5–21. https://doi.org/10.1016/0378-3804(82)90016-X.
[14] Liu, T., Wang, Y., Wu, J., Xia, X., Wang, J., et al., 2015, Springback analysis of Z & T-section 2196-T8511 and 2099-T83 Al-Li alloys extrusions in displacement controlled cold stretch bending. Journal of Materials Processing Technology, 225:295–309. https://doi.org/10.1016/j.jmatprotec.2015.05.024.
[15] Paulsen, F., Welo, T., 2001, Cross-sectional deformations of rectangular hollow sections in bending: part II - analytical models. International Journal of Mechanical Sciences, 43/1:131–152. https://doi.org/10.1016/S0020-7403(99)00107-1.
[16] Zhu, H., Stelson, K.A., 2002, Distortion of rectangular tubes in stretch bending. Journal of Manufacturing Science and Engineering, Transactions of the ASME, 124/4:886–890. https://doi.org/10.1115/1.1511170.
[17] Liu, J.H., Francis, A., 2004, Theoretical analysis of local indentation on pressured pipes. International Journal of Pressure Vessels and Piping, 81/12:931–939. https://doi.org/10.1016/j.ijpvp.2004.05.007.
[18] Chang, Z., Li, M., Chen, J., 2019, Analytical modeling and experimental validation of the forming force in several typical incremental sheet forming processes. International Journal of Machine Tools and Manufacture, 140:62–76. https://doi.org/10.1016/j.ijmachtools.2019.03.003.
[19] Holstein, V., Hermes, M., Tekkaya, A.E., 2020, Analysis of incremental die bending of wires and tubes. Production Engineering, 14/2:265–274. https://doi.org/10.1007/s11740-020-00952-1.
[20] Ma, J., Welo, T., Ringen, G., 2021, Efficient prediction of real-time forming forces in flexible stretch bending. ESAFORM2021, 10:1–11.